

A mmWave Oscillator Design Utilizing High-Q Active-Mode On-Chip MEMS Resonators for Improved Fundamental Limits of Phase Noise

Abhishek Srivastava, *Senior Member, IEEE*, Baibhab Chatterjee,, *Graduate Student Member, IEEE*,
Udit Rawat, *Graduate Student Member, IEEE*, Yanbo He, *Member, IEEE*, Dana Weinstein, *Senior Member, IEEE*,
and Shreyas Sen, *Senior Member, IEEE*

Abstract—Recent progress in MEMS resonant-fin-transistors (RFT) allows very high-Q active mode resonators, promising crystal-less monolithic clock generation for mmWave systems. However, there is a strong need for design of mmWave oscillators that utilize the high-Q of active-mode RFT (AM-RFT) optimally, while handling unique challenges such as resonator's low electromechanical transduction. In this brief, we develop a theory and through design and post-layout simulations in 14-nm Global Foundry process, we show the first active oscillator with AM-RFT at 30 GHz, which improves the fundamental limits of phase noise and figure-of-merit as compared to the oscillators with conventional LC resonators. For AM-RFT with Q-factor of 10K, post layout simulation results show that the proposed oscillator exhibits phase noise < -140 dBc/Hz and figure-of-merit > 228 dBc/Hz at 1 MHz offset for 30 GHz center frequency, which are > 25 dB better than the existing monolithic LC oscillators.

Keywords—Oscillator, mmWave, MEMS, phase-noise, 14 nm

I. INTRODUCTION

Utilization of mmWave spectrum (> 20 GHz) in 5G communication technologies for increased data rates (upto 4 Gb/s) requires large arrays of wireless transceivers in multiple-input-multiple-output (MIMO) fashion [1]. For cost effective and area efficient mmWave carrier generation in MIMO systems, it requires more versatile resonators with monolithic IC integration capabilities at mmWave frequencies as compared to the conventional phase locked loop (PLL) based carrier synthesis, which needs bulky and costly off-chip piezoelectric quartz crystals. With the advancements in micro-electro-mechanical systems (MEMS) technologies, such as MEMS-First, MEMS-Last [2], Back-End-Of-Line MEMS [3] and Acoustic Bragg Reflectors (ABR) [4], it seems viable to satisfy the demands of fully monolithic mmWave carrier synthesis.

Traditional MEMS resonators utilize passive electrostatic or piezoelectric transduction schemes, and exhibit low electromechanical transduction and high parasitic feed-through, which can be mitigated by active FET sensing techniques [5]. In our previous work [6], we utilized active FET sensing and demonstrated a very high-Q, active mode Resonant Fin Transistor (AM-RFT) using ABR technique. AM-RFT was fabricated in Global Foundry's 14nm FinFET technology, leveraging the vertical 3D geometry of FinFETs to efficiently confine, drive, and sense acoustic vibrations in the solid (unreleased) CMOS stack. In this work, we utilize high-Q active-mode MEMS resonator to develop an oscillator for fully monolithic

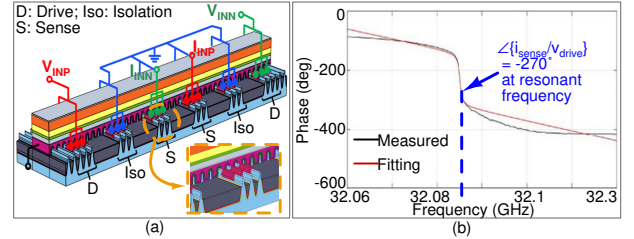


Fig. 1: (a) RFT unit cell showing differential driving voltage for a 3-skip-4 fin connections, (b) measured phase shift between output (sensed) current and input (drive) voltage [6]

mmWave carrier synthesis, for which we present - 1) a novel oscillator topology with active-mode MEMS resonator, which improves the existing fundamental limits of phase noise and figure-of-merit (FoM) obtained from LC oscillators, 2) an electrical model of voltage-driven, current-sensed high-Q on-chip active-mode MEMS resonator for circuit simulation, 3) an analysis for phase noise of the proposed oscillator and 4) verification of the proposed topology with the design and simulation of a 30 GHz oscillator in 14-nm GF process. In this brief, AM-RFT has been used to explain the techniques proposed, however, the insights presented can be in general applied for any high-Q on-chip active-mode MEMS resonator.

The paper is organised as follows. Section II presents the device structure and electrical model of AM-RFT. Sections III and IV present the proposed oscillator topology and its phase noise analysis, respectively. Section V presents the implementation details with post-layout simulation results followed by the conclusion of the paper.

II. ACTIVE MODE MEMS RESONATOR

A. Device structure

The central section of the complete AM-RFT cavity is shown in Fig.1(a). Multiple pairs of drive MOSCAP transducer units are used for converting the input voltage capacitively into the actuation force. Each unit consists of a 3-fin MOSCAP with the Gate forming one of the plates and the shorted Source-Drain forming the other. The respective phases of the differential signal are applied to the shorted Source-Drains of the the drive units. To satisfy the DRC constraints 4 fins are skipped between every pair of units. Once the resonance modes are excited by applying the differential input actuation voltage, the vibrating fins exhibit periodically varying mechanical stress. The periodic stress modulates the drain

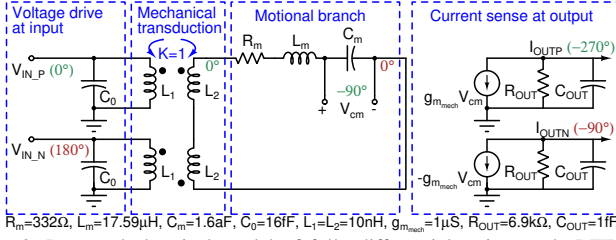


Fig. 2: Proposed electrical model of fully differential active mode RFT for circuit simulations

current flowing through the 3-fin sense transistors resulting in a differential output (due to opposite phases of stress at the sense transistor fins). A Phase shift of 90° results for the transformation from electrical to mechanical domain. Subsequently, the output current of the sense transistors in conjunction with their output resistances causes an additional phase shift of 180° . Essentially, ABR based active mode resonators act as a voltage controlled current source with 270° phase shift (VCCS₂₇₀) between the input (driving) voltage and the output (sensed) drain current. Fig.1(b) also shows that the measured phase shift for AM-RFT is 270° [6].

B. Electrical Model for Active Mode RFT

Fig. 2 depicts the proposed electrical model for fully differential VCCS₂₇₀ realization of AM-RFT. R_m , L_m and C_m are the motional resistance, inductance and capacitance, respectively, which model the resonant behaviour of the device with resonant frequency $f_0 = \frac{1}{2\pi\sqrt{L_m C_m}}$ [7], [8]. C_0 is the static capacitance at the driving ports [6] and $g_{m_{mech}}$ is the transconductance showing relation between sensed drain current (I_{OUT}) and voltage across C_m (V_{cm}). R_{OUT} and C_{OUT} are the output resistance and capacitance at the drain terminal of the sensing FET, respectively. Fig. 2 also shows the parameters of the proposed electrical model of 30 GHz AM-RFT with $Q = 10,000$ [6], where C_0 , $g_{m_{mech}}$, R_{OUT} and C_{OUT} were evaluated with the help of AC simulations of the layout extracted netlist of the RFT device. For evaluating C_m , sufficiently small electromechanical coupling coefficient ($\frac{C_m}{C_0}$) of 10^{-4} was considered for AM-RFT. In AM-RFT, the motional branch directly appears at the driving port due to the mechanical transduction [5]. Therefore, as shown in Fig. 2, mechanical transduction is modelled with mutually coupled inductors L_1 and L_2 having coupling co-efficient (K) as 1, because any other value of K will modify the impedances of the driving port and the motional branch due to the transformer action between L_1 and L_2 . It is also important to select $L_1 = L_2 \ll L_m$ such that f_0 is not changed and voltage drop across L_1 and L_2 is negligible as compared the drop across the motional branch. At the same time L_1 and L_2 should be large enough such that they do not load the drive input. Considering these facts, $L_1 = L_2 = 10$ nH is chosen as shown in Fig. 2.

The model shown in Fig. 2 helps in topological evolution and simulations of oscillator circuits for active-mode resonators. Now two questions arise - 1) how can an active-mode resonator, realised as VCCS₂₇₀, be utilized to build an oscillator and 2) will there be any advantage in the oscillator phase noise as compared to the conventional LC oscillators. These questions are addressed in sections III and IV, respectively.

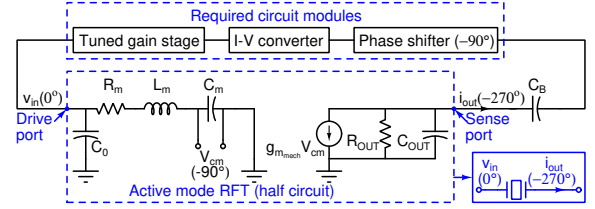


Fig. 3: Depiction of required circuit modules to build oscillator with half circuit model of VCCS₂₇₀ realization of AM-RFT in a feedback loop

III. OSCILLATOR CIRCUIT TOPOLOGY

To build an oscillator with VCCS₂₇₀ realization of the resonator, Barkhausen criteria must be met in a feedback loop, for which the phase shift around the closed loop should be 0° and the loop gain must be ≥ 1 . Fig. 3 depicts the oscillator block diagram with the help of the half circuit model of VCCS₂₇₀. As shown in Fig. 3, the circuit requires a phase shifter for the additional -90° phase shift and an I-V conversion stage to convert the current sensed from the output of VCCS₂₇₀ into voltage, which can be fed back to its input drive port. Moreover, as shown in Fig. 3, for meeting the loop-gain criteria at 30 GHz, a tuned narrowband gain stage is also needed in the loop. Realization techniques for phase-shifter and I-V converter, and the order in which the required blocks are placed in the loop lead to different topological choices, which are discussed in the following subsection.

A. Topology choices

Fig. 4 presents three techniques to achieve additional 90° phase shift and the corresponding oscillator topologies, which are discussed below.

a) *Gain-stage-first with a series RLC phase shifter*: Fig. 4(a) depicts the first method, where -90° phase shift can be obtained at resonance by using a series $R_s L_s C_s$ network. Fig. 4(b) depicts the oscillator topology with a gain-stage-first approach with the series $R_s L_s C_s$ network as phase-shifter, where C_0 of the resonator is utilized as C_s . This topology requires a cascade of two tuned gain stages, to provide high gain at 30 GHz, along with an active I-V converter in order to maintain the phase criteria in the loop, which considerably increases power, area and circuit complexity. Therefore, it is not a preferable choice.

b) *Capacitor as a phase shifter and I-V converter*: Fig. 4(c) shows the second method, where a capacitor (C_ϕ) is used to provide the phase shift of -90° while also doing the I-V conversion. Fig. 4(d) depicts the topology with C_ϕ followed by cascade of two tuned gain stages. As compared to the first topology shown in Fig. 4(b), it does not need an explicit I-V converter and hence is a better choice. However, it also needs cascaded tuned stages, which demands for high power consumption, therefore, a lower power alternate must be explored, which is the third method discussed next.

c) *Inductor as a phase shifter and I-V converter*: Fig. 4(e) shows the third method where an inductor is used to provide 90° phase-shift and I-V conversion simultaneously. Fig. 4(f) depicts the oscillator topology for this technique. To meet the phase shift and gain criteria in the loop, this topology needs a single tuned gain stage. It is a lower power choice as

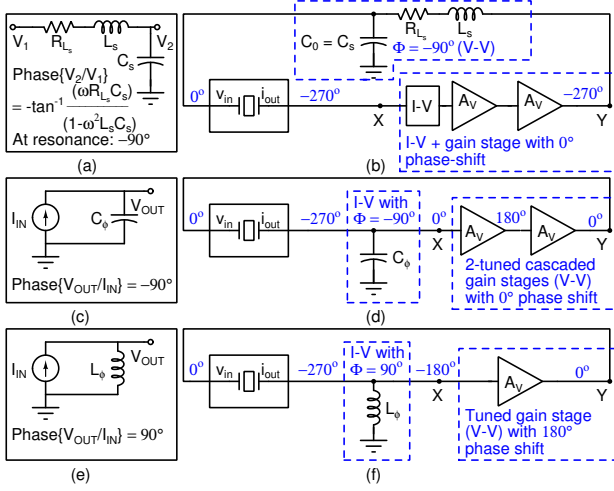


Fig. 4: Methods to provide 90° phase shift and corresponding oscillator topology choices. (a)-(b) using a series RLC as phase shifter, (c)-(d) using a capacitor as phase shifter and (e)-(f) using an inductor as phase shifter

compared to C_ϕ method shown in Fig. 4(d) as it requires less stages. Therefore, this topology has been chosen to build the oscillator with high-Q on-chip active mode MEMS resonator, which is discussed in detail in the following subsection.

B. Proposed oscillator topology

Fig. 5 shows the schematic of the proposed oscillator topology, where L_ϕ provides the desired 90° phase shift and I-V conversion. For the tuned gain stage, a common source stage is used where the static capacitance (C_0) of AM-RFT has been utilized in its load tank with an inductor L_0 having a loss resistance R_{L_0} and Q-factor $Q_{L_0} = \frac{\omega L_0}{R_{L_0}}$. At mmWave frequencies, the impedance of C_0 ($X_{C_0} = \frac{1}{j\omega C_0}$) becomes comparable to R_m and ac signal flows to the ac ground through it, which considerably increases the drive requirements of the oscillator. This is a critical problem with on-chip MEMS resonators [9], which is solved in the proposed topology by including C_0 in the resonant tank of the tuned gain stage.

It is important that at f_0 , the phase-shifter L_ϕ does not resonate with C_{in} , which is the total capacitance due to the routing parasitics and the input of the gain stage M_1 (Fig. 5), otherwise it will cease to provide 90° phase shift. In fact, the resonant frequency ($f_\phi = \frac{1}{2\pi\sqrt{L_\phi C_{in}}}$) of the $L_\phi C_{in}$ tank should be much larger than f_0 , which gives the maximum limit of L_ϕ as shown in (1).

$$\frac{1}{2\pi\sqrt{L_\phi C_{in}}} \gg f_0 \Rightarrow L_\phi \ll \frac{1}{4\pi^2 f_0^2 C_{in}} \quad (1)$$

From Fig. 5, gain of tuned stage $A_{V1} = \frac{v_Y}{v_X}$ can be given by (2), while its load tank is tuned near f_0 .

$$A_{V1} = \frac{v_Y}{v_X} = (g_{m_{M1}} \times R_0)^2 \quad (2)$$

In (2), $g_{m_{M1}}$ is the transconductance of M_1 , $R_0 = R_m \parallel (Q_{L_0}^2 \times R_{L_0}) \parallel r_{o_{M1}}$ and $r_{o_{M1}}$ is the small signal output resistance of M_1 . From Fig. 5, $v_X \approx g_{m_{mech}} v_{cm} \times |\omega_0 L_\phi| = g_{m_{mech}} \frac{v_Y}{\omega C_m} \times \frac{1}{\omega C_m} \times |\omega_0 L_\phi|$, which gives $A_{V2} = \frac{v_X}{v_Y}$ shown in Eq. (3).

$$A_{V2} = \frac{v_X}{v_Y} = \frac{g_{m_{mech}} L_\phi}{C_m R_m} \quad (3)$$

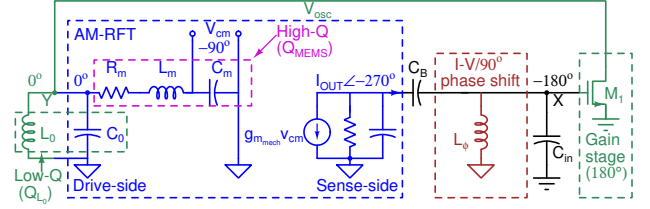


Fig. 5: Schematic of the proposed oscillator circuit

For oscillations to build up at f_0 , $A_{V1} \times A_{V2} > 1 \Rightarrow (g_{m_{M1}} \times R_0)^2 \times \frac{g_{m_{mech}} L_\phi}{C_m R_m} > 1$, which gives expression for minimum L_ϕ (4).

$$L_\phi \gg \frac{R_m C_m}{g_{m_{mech}} (g_{m_{M1}} \times R_0)^2} \quad (4)$$

Equations (1) and (4) together suggests the suitable start value for L_ϕ , which can be further optimized through simulations.

As shown in Fig. 5, there are two resonant tanks in the proposed circuit- 1) High-Q ($Q_{MEMS}=10K$) $R_m L_m C_m$ tank and 2) Low-Q ($Q_{L_0} < 30$) $L_0 C_0$ tank. With two tanks in the loop, a fundamental question arises for the proposed topology - is there any improvement in the phase noise as compared to the conventional LC oscillators. To answer this question, phase noise analysis for the proposed oscillator is discussed in the following section.

IV. PHASE NOISE PERFORMANCE OF THE PROPOSED AM-RFT BASED OSCILLATOR

Phase noise ($\mathcal{L}\{\Delta\omega\}$) in dBc/Hz of an oscillator at an offset ($\Delta\omega$) from a frequency ω_0 can be defined as follows.

$$\mathcal{L}\{\Delta\omega\} = 10 \log \frac{P_n(\Delta\omega)}{P_c} \quad (\text{dBc/Hz}) \quad (5)$$

where, $P_n(\Delta\omega)$ is the noise power spectral density at $\Delta\omega$ and $P_c = \frac{V_{OSC}^2}{2}$ is the carrier power at ω_0 with oscillation amplitude V_{OSC} . The noise spectrum experiences filtering due to the two resonant circuits present in the loop (Fig. 5), which governs the phase noise performance of the proposed oscillator. For modelling the phase noise, effective noise power and its filtering due to the overall Q-factor of the oscillator (Q_{OSC}) are discussed below.

a) *Noise power (P_n) sources in the loop:* As shown in Fig. 6(a), there are five major noise sources in the oscillator: 1) $V_{n_{R_m}}^2$ due to R_m , 2) $V_{n_{R_{L_0}}}^2$ due to R_{L_0} , 3) $V_{n_{g_{m_{M1}}}}^2$ due to the gain stage's output noise 4) $V_{n_{g_{m_{mech}}}}^2$ due to the sense transistor's output noise and 5) $V_{n_{R_{L_\phi}}}^2$ due to R_{L_ϕ} , which are lumped into two noise sources N_1 and N_2 at nodes X and Y, respectively. Noise from R_{L_0} and transistor's channel noise appear directly at the oscillator output. Moreover, impedance reflection (1:1) at input of AM-RFT due to the transformer action, also causes R_m noise to appear at the oscillator output. Gain stage amplifies the total noise present at its input, which is due to the sense transistor's channel noise and thermal noise of R_{L_ϕ} . The total noise power at the oscillator output can be given by Eq. (6).

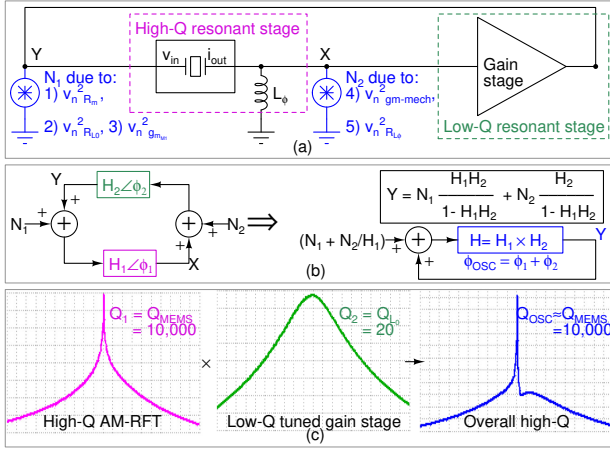


Fig. 6: (a) Noise sources in the oscillator, (b) depiction of two resonant stages in the positive feedback loop of the proposed oscillator (c) simulation showing overall Q-factor of the oscillator is approximately same as the Q_{MEMS}

$$P_n = \left(\frac{4kT}{R_m} + \frac{4kT}{R_{L0}} + 4kT\gamma g_{m_{M1}} \right) R_0^2 + A_{v1}^2 \left(4kT\gamma g_{m_{mech}} + \frac{4kT}{R_{L\phi}} \right) R_{L\phi}^2 \quad (6)$$

b) Overall Q-factor and effective noise power: As shown in the Fig. 6(b), the two LC resonant circuits are cascaded, therefore their frequency responses get multiplied in the loop ($H(s) = H_1(s) \times H_2(s)$) resulting into an overall phase shift (ϕ_{OSC}) given by Eq. (7), which is the sum of phase shifts of the two networks.

$$\phi_{OSC} = \phi_1 + \phi_2 \quad (7)$$

Since $Q = \frac{\omega_0}{2} \left| \frac{d\phi}{d\omega} \right|$ [10], therefore, from Eq. (7) the overall Q of the oscillator (Q_{OSC}) can be given by Eq. (8).

$$Q_{OSC} = Q_{L0} + Q_{MEMS} \approx Q_{MEMS} \quad (8)$$

Fig. 6(c) depicts the simulated frequency responses of the two resonant tanks and their combined response, which also shows that $Q_{OSC} \approx Q_{MEMS}$ near resonant frequency. It is important to note that the circuit has two distinct resonant circuits, which might have slight mismatch in their resonant frequencies due to parasitics and fabrication process. However, coupling of the mechanical vibrations through high-Q ($Q_{MEMS} \gg Q_{L0}$) AM-RFT at f_0 will result into the sustained oscillations closer to f_0 with $Q_{OSC} \approx Q_{MEMS}$. For the feedback system shown in Fig. 6(b), $\frac{Y}{N} = \frac{H}{1-H}$, with very high Q_{OSC} and $|H| \approx 1$ near ω_0 , which gives $\left| \frac{d\phi}{d\omega} \right|^2 \gg \left| \frac{dH}{d\omega} \right|^2$ leading to Leeson's heuristic expression $\left| \frac{Y}{N} \right|^2 = \left(\frac{\omega_0}{2Q_{OSC}\Delta\omega} \right)^2$ for the proposed topology [11]. Using Leeson's expression, $P_n(\Delta\omega)$ at an offset of $\Delta\omega$ from ω_0 can be given as follows.

$$P_n(\Delta\omega) = \left(\frac{\omega_0}{2Q_{OSC}\Delta\omega} \right)^2 P_n \quad (9)$$

From Eq. (5) and Eq. (9), due to very high Q_{OSC} , noise filtering is maximized near resonant frequency, which considerably improves the phase noise of the oscillator.

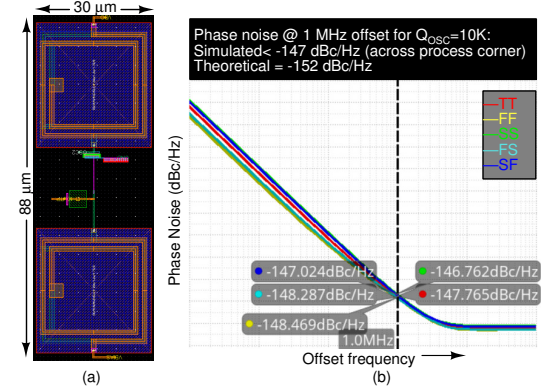


Fig. 7: (a) Layout of the proposed oscillator, (b) post-layout simulation results of PN across process corners showing close agreement with the theoretical model

c) Phase noise expression: Noise factor of oscillator (F), which is defined as the total oscillator phase noise normalized to phase noise due to the MEMS resonator loss (R_m), can be calculated by dividing (6) by $\frac{4kT}{R_m} R_0^2$ and shown in (10).

$$F = 1 + \frac{R_m}{R_{L0}} + \gamma g_{m_{M1}} R_m + \gamma g_{m_{mech}} g_{m_{M1}}^2 R_m R_{L\phi}^2 + g_{m_{M1}}^2 R_m R_{L\phi} \quad (10)$$

where, k is the Boltzmann's constant and T is the temperature in Kelvin. Using equations (5) and (9), phase noise of the oscillator in dBc/Hz can be given by the following expression.

$$\mathcal{L}\{\Delta\omega\} = 10 \log \left\{ F \frac{4kTR_0^2}{R_m \times V_{OSC}^2} \left(\frac{\omega_0}{2Q_{OSC}\Delta\omega} \right)^2 \right\} \quad (11)$$

Theoretical minimum phase noise of the proposed oscillator can be calculated by considering the noise due to R_m only, for which $F = F_{min} = 1$. Considering, $R_0 = R_m = 332 \Omega$, $Q_{OSC} = 10K$, $\omega_0 = 30$ GHz, $\Delta\omega = 1$ MHz, $V_{OSC} = V_{DD} = 800$ mV, the theoretical minimum phase noise is $\mathcal{L}\{\Delta\omega\} = -167$ dBc/Hz. This significantly low phase noise is a manifestation of effective utilization of high Q factor of the active-mode resonator.

V. IMPLEMENTATION AND SIMULATION RESULTS

The proposed circuit (Fig. 5(c)) has been implemented in 14 nm GF technology and post-layout simulations were performed on the design. Fig. 7(a) shows the layout of the circuit, which occupies an area of $88\mu m \times 30\mu m$. In the design, $L_0 = 650$ pH with $Q_{L0} \approx 10$ and $R_{L0} \approx 13\Omega$, and $L_\phi = 650$ pH, which satisfies equations (1) and (4). Moreover, L_ϕ with the extracted value of $C_{in} \approx 5$ fF, makes $f_\phi = \frac{1}{2\pi\sqrt{L_\phi C_{in}}} = 88$ GHz $\gg f_0$ (30 GHz), and thus provides 90° phase shift with I-V conversion. For the designed M_1 , $g_{m_{M1}} \approx 15$ mA/V. Electrical parameters of AM-RFT shown in Fig. 2 were used for oscillator simulations. The total power consumption (P_{DC}) is 5.7 mW from 800 mV supply.

Fig. 7(c) shows that the post-layout simulated phase noise at 1 MHz offset (PN) is < -146 dBc/Hz across the process corners. With the values mentioned earlier and from Eq. (10), $F=32.3$, which gives a theoretical value of PN ≈ -151.6

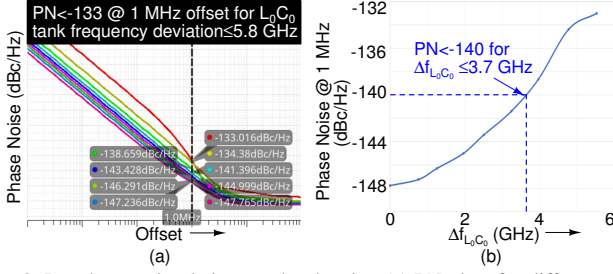


Fig. 8: Post-layout simulation results showing (a) PN plots for different (than f_0) resonant frequencies of L_0C_0 tank (b) $PN < -140$ dBc/Hz for $\Delta f_{L_0C_0} \leq 3.7$ GHz

TABLE I: Performance summary and comparison

Parameters	[12]	[13]	[14]	[15]	This work
Measured/ Simulated	Measured	Measured	Measured	Measured	Simulated (post-layout)
Technology	180 nm CMOS	40 nm CMOS	65 nm CMOS	65 nm CMOS	14 nm CMOS
Frequency	17 GHz	30.7 GHz	28 GHz	29.92 GHz	30 GHz
Resonator	Switched- interdigital	Dual LC	Dual-path L & C	Multi-resonant RLCM	Active-Mode MEMS [6]
PN (dBc/Hz) @1MHz	-105	-104.98	-102.5†	-112.31	<-140
Power	7.2 mW	>9 mW	4.7 mW	4 mW	5.7 mW
FoM (dBc/Hz)‡	182	<184.4	<184.5	<189.8	228
Supply	1.8 V	1.1 V	1.2 V	0.48 V	0.8 V
Die-Area (mm ²)	0.34	0.08	0.0875	0.08	0.0026

†Taken from the graph in the paper. ‡ $FoM = (\frac{f_0}{\Delta f})^2 / (\mathcal{L}\{\Delta f\} P_{DC}) \times 10^{-3}$

dBc/Hz (Eq. (11)), which is not too far from the simulated value of -147.8 dBc/Hz at TT as shown in Fig. 7(b). FoM of the proposed oscillator is about 228 dBc/Hz. Fig. 8(a) shows PN plots when resonant frequency of L_0C_0 tank deviates with respect f_0 . As depicted in Fig. 8(b), PN is better than -140 dBc/Hz for frequency deviations ($\Delta f_{L_0C_0}$) upto 3.7 GHz. This shows that the high-Q AM-RFT is able to sustain the oscillations by pulling the slight variations in L_0C_0 tank frequency to close to f_0 . Table I shows the performance summary of the proposed oscillator and its comparison with other works, which conveys the fact that as compared to the oscillators with LC-tank resonators near 30 GHz, it is possible to utilize the high-Q of an active-mode monolithic MEMS resonator and build oscillators with significantly improved (> 25 dB) PN and FoM.

CONCLUSIONS

In this research a novel, low phase noise, monolithic oscillator topology has been presented with a high-Q active-mode MEMS resonator, which acts as a VCCS having 270° phase shift between its output current and input voltage. Supported with analysis, important insights have been presented in this brief, which indicate that the fundamental limits of PN and FoM for mmWave oscillators can be improved by >25 dB with monolithic active-mode MEMS resonators as compared to the conventional LC tank resonators. The proposed topology is verified with the design and post layout simulations of the first 30 GHz oscillator with active mode resonator in 14-nm GF process. Post layout simulation results show that the proposed oscillator with active mode resonator having $Q = 10K$, exhibits phase noise < -140 dBc/Hz and FoM > 228 dBc/Hz at 1 MHz offset for 30 GHz center frequency, which are >25 dB better as compared to the existing monolithic LC oscillators.

ACKNOWLEDGEMENT

Authors acknowledge DARPA MIDAS program for funding this research work.

REFERENCES

- [1] J. S. Herd and M. D. Conway, "The Evolution to Modern Phased Array Architectures," *Proceedings of the IEEE*, vol. 104, no. 3, pp. 519–529, 2016.
- [2] G. K. Fedder, R. T. Howe, T. K. Liu, and E. P. Quevy, "Technologies for Cofabricating MEMS and Electronics," *Proc. of the IEEE*, vol. 96, no. 2, pp. 306–322, Feb 2008.
- [3] C. Li, L. Hou, and S. Li, "Advanced CMOS-MEMS Resonator Platform," *IEEE Electron Device Letters*, vol. 33, no. 2, pp. 272–274, Feb 2012.
- [4] W. E. Newell, "Face-mounted piezoelectric resonators," *Proc. of the IEEE*, vol. 53, no. 6, pp. 575–581, June 1965.
- [5] B. Bahr, R. Marathe, W. Wang, and D. Weinstein, "Solid state rf mems resonators in standard cmos," in *2013 Proceedings of the ESSCIRC (ESSCIRC)*, 2013, pp. 249–252.
- [6] B. Bahr, Y. He, Z. Krivokapic, S. Banna, and D. Weinstein, "32GHz resonant-fin transistors in 14nm FinFET technology," in *2019 IEEE International Solid- State Circuits Conference - (ISSCC)*, Feb 2018, pp. 348–350.
- [7] S. Gong and G. Piazza, "Design and analysis of lithium-niobate-based high electromechanical coupling rf-mems resonators for wideband filtering," *IEEE Transactions on Microwave Theory and Techniques*, vol. 61, no. 1, pp. 403–414, 2013.
- [8] G. Piazza, P. J. Stephanou, and A. P. Pisano, "Piezoelectric aluminum nitride vibrating contour-mode mems resonators," *Journal of Microelectromechanical Systems*, vol. 15, no. 6, pp. 1406–1418, 2006.
- [9] A. Srivastava, B. Chatterjee, U. Rawat, Y. He, D. Weinstein, and S. Sen, "Analysis and Design Considerations for Achieving the Fundamental Limits of Phase Noise in mmWave Oscillators with On-Chip MEMS Resonator," *IEEE Transactions on Circuits and Systems II: Express Briefs*, pp. 1–1, 2020.
- [10] B. Razavi, "A study of phase noise in CMOS oscillators," *IEEE Journal of Solid-State Circuits*, vol. 31, no. 3, pp. 331–343, 1996.
- [11] D. B. Leeson, "A Simple Model of Feedback Oscillator Noise Spectrum," *Proc. IEEE*, no. 2, p. 329–330, Feb 1966.
- [12] I. Mansour, M. Aboulalaa, A. Allam, A. B. Abdel-Rahman, M. Abo-Zahhad, and R. K. Pokharel, "Dual Band VCO Based on a High-Quality Factor Switched Interdigital Resonator for the Ku Band Using 180-nm CMOS Technology," *IEEE Transactions on Circuits and Systems II: Express Briefs*, vol. 65, no. 12, pp. 1874–1878, 2018.
- [13] Y. Shu, H. J. Qian, and X. Luo, "A 18.6-to-40.1GHz 201.7dBc/Hz FoMT Multi-Core Oscillator Using E-M Mixed-Coupling Resonance Boosting," in *2020 IEEE International Solid- State Circuits Conference - (ISSCC)*, 2020, pp. 272–274.
- [14] M. A. Hoque, M. Chahardori, P. Agarwal, M. A. Mokri, and D. Heo, "Octave Frequency Range Triple-band Low Phase Noise K/Ka-Band VCO with a New Dual-path Inductor," in *2020 IEEE/MTT-S International Microwave Symposium (IMS)*, 2020, pp. 341–344.
- [15] H. Guo, Y. Chen, P. Mak, and R. P. Martins, "A 0.08mm² 25.5-to-29.9GHz Multi-Resonant-RLCM-Tank VCO Using a Single-Turn Multi-Tap Inductor and CM-Only Capacitors Achieving 191.6dBc/Hz FoM and 130kHz 1/f³ PN Corner," in *2019 IEEE International Solid- State Circuits Conference - (ISSCC)*, 2019, pp. 410–412.